MODELING TECHNIQUES FOR DESIGN AND ANALYSIS OF SUPERCONDUCTING ACCELERATOR MAGNETS*

P. Ferracin, LBNL, Berkeley, CA 94720, USA

Abstract

Superconducting magnets for particle accelerators are complex devices requiring the use of sophisticated modelling techniques to predict their performance. A complete description of the magnet behaviour can only be obtained through a multi-physics approach which combines magnetic models, to compute magnetic fields and electro-magnetic forces, mechanical models, to study stresses arising during assembly, cool-down and excitation, and electrical-thermal models, to investigate temperature margins and quench phenomena. This approach is essential in particular for the next generation of superconducting accelerator magnets, which will likely implement strain sensitive conductors like Nb_3Sn and will handle forces significantly larger than in the present LHC dipoles. The design of high field superconducting magnets has benefited from the integration between CAD, magnetic, and structural analysis tools allowing a precise reproduction of the magnet 3D geometry and a detailed analysis of the three-dimensional strain in the superconductor. In addition, electrical and thermal models have made possible investigating the quench initiation process and the thermal and stress conditions of the superconducting coil during the propagation of a quench. We present in this paper an overview of the integrated design approach and we report on simulation techniques aimed to predict and improve magnet behaviour.

INTRODUCTION

The R&D on the next generation of superconducting magnets for particle accelerators is currently focused on quadrupoles and dipoles for future luminosity and energy upgrades of the LHC [1]. Other possible applications include neutrino factories and cable test facilities [2]. These magnets will operate at field approaching 15 T, i.e. beyond the limits of NbTi superconductor, and with stored energies and electro-magnetic (e.m.) forces significantly larger than in the magnets presently used in the LHC. At the moment, Nb_3Sn, the only practical superconductor capable of generating fields higher than 10 T, appears as the best candidate for this future generation of superconducting magnets. However, Nb_3Sn is a brittle and strain-sensitive superconductor whose current carrying capability depends on its strain status [3,4]. As a result, the performance of Nb_3Sn magnets can be strongly affected by the mechanical stresses in the windings during magnet operation. It is therefore mandatory to understand and predict the strain in the superconductor, and devise a support structure capable of minimizing the stresses in the coils from magnet assembly to excitation.

The computation of the mechanical status of the superconducting material is a very complex task, considering all the stages involved in the fabrication of Nb_3Sn coils, like cabling, winding, heat treatment to 650 °C, and epoxy impregnation (Fig. 1). These steps are then followed by magnet assembly, pre-loading, cool-down and powering, which further contribute to the final strain conditions of the Nb_3Sn superconductor.

Figure 1: Nb_3Sn coil after winding (left), after reaction (center), and after impregnation (left).

We present in this paper an overview on modelling works performed in the LBNL Superconducting Magnet Program and aimed at design Nb_3Sn superconducting magnets, predict their behaviour, and analyze and improve quench performance. We start with a description of the tools and techniques adopted, and we then discuss how the models can be used to optimize coil and magnet lay-outs, improve fabrication process, and predict and minimize coil stress from assembly to quench.

INTEGRATED MODELING: TOOLS AND TECHNIQUES

The design and analysis of superconducting magnets can be seen as one single process that integrates different tools to provide a full characterization of the magnet components during assembly, cool-down, magnet excitation and quench. We present in this section an overview of codes and techniques utilized for superconducting magnet design, starting from simplified scaling laws to full 3D magnet models. A complete description of the integrated design approach applied to accelerator magnets can be found in [5].

Coil and Magnet 2D Design

The first step of magnet design consists in a preliminary estimate, through analytical tools or scaling laws, of the amount of conductor required for a given field and aperture [6-8]. Then, the definition of a 2D cross-section of superconducting cable, coil and support structure constitutes the second design step. In this phase, a 2D analysis of the magnetic and mechanical behaviour of the magnet can be performed with programs like Poisson [9], Roxie [10], Opera 2D [11] and ANSYS [12] (Fig. 3). The output of such programs gives field, harmonics and short-sample predictions for the magnet performance, as well as stress in all magnet components.
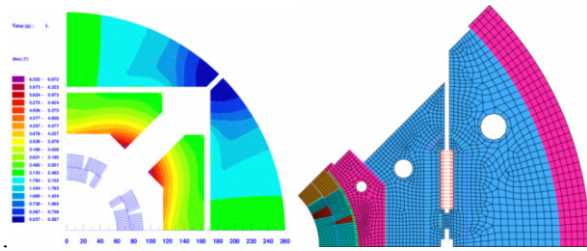
Figure 3: 2D finite element model for magnetic (Roxie, left) and mechanical (ANSYS, right) analysis.

Coil 3D Design

With the optimized coil cross-section coordinates, it is then possible to proceed and complete the cable windings through return and lead ends, using computer programs such as Bend [13] and Roxie. The resulting full 3D model of the coil, including each individual turn (Fig. 4), can be then uploaded in CAD programs, like ProE [14], for the coil parts fabrication, or in Opera 3D and ANSYS for magnetic and mechanical analysis (Fig. 5).
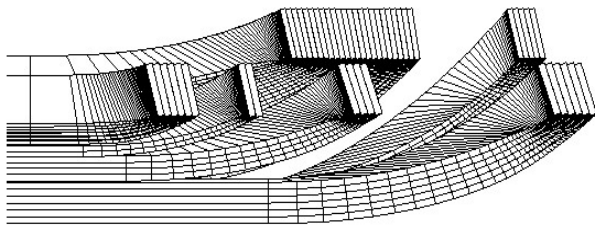

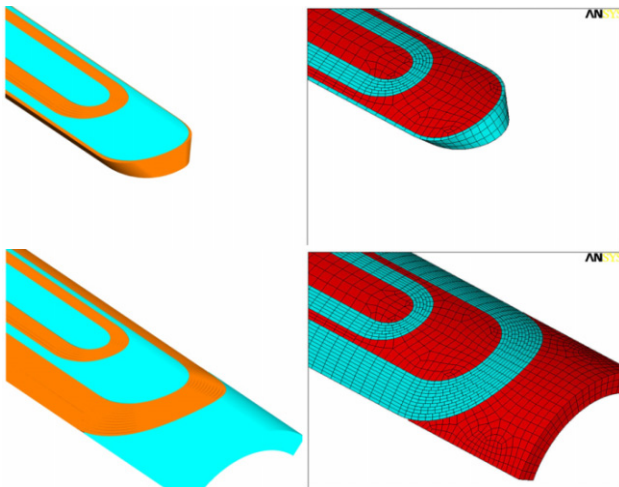Figure 4: 3D coil model generated by the program Bend.

Figure 5: 3D coil model imported in ProE (left) and ANSYS (right).

Magnet 3D Design

At this point, the final step consists in the implementation of the full 3D magnet geometry. The CAD models are used to define assembly and loading procedures, and to generate drawings for part fabrication. Opera 3D and Roxie models compute conductor peak fields in the coil ends, and optimize iron geometry and field quality in the end regions (Fig. 6). Finally, an ANSYS 3D model can focus on the design of the support structure, with particular emphasis on the coil axial

support system. The integration of all these programs will have as an output a full description of the magnetic, mechanical and thermal condition of the superconductor, and will provide fundamental information to analyze magnet performance, identify quench triggering mechanisms, and define corrective strategies to improve training and minimize stress in the superconductor.
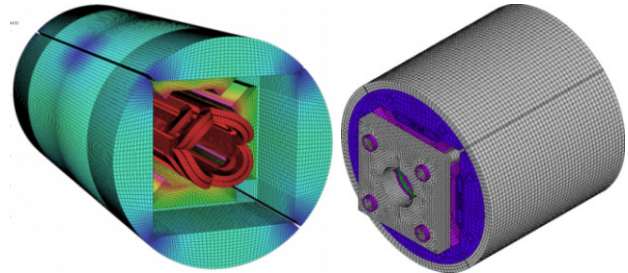

Figure 6: 3D finite element model for magnetic (Vector Field, left) and mechanical (ANSYS, right) analysis.

COIL AND SUPPORT STRUCTURE DESIGN

In Nb_3Sn magnets, the risk of conductor degradation due to high stress requires that already from the initial phases of the design, aimed at defining the 2D coil and magnet cross-sections, one of the main objectives must be minimizing the accumulated stress on the conductor. At the same time, the support structure must provide enough coil pre-load after cool-down so that turns do not separate from coil parts when the e.m. forces start to act on the windings. We present in this section the results of a conceptual design study focused at the optimization of the coil and support structure cross-sections of quadrupoles.

Coil Cross-Section Optimization

In a shell-type coil, the e.m azimuthal forces are directed towards the mid-plane, where the accumulated stress reaches its peak at high field. In a multi-layer coil configuration, the choice of the number of turns per layer can play a significant role in reducing the accumulated stresses.
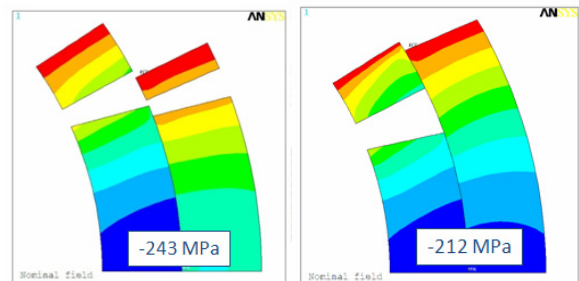

Figure 7: 2D computations of azimuthal stress with e.m. forces. Red (blue) contours indicate area of low (high) compressive stress.

In Fig. 7 we plotted the stress at maximum field of two different coil designs considered for the LHC Accelerator Research Program (LARP) quadrupole magnet HQ

[15,16]. In the first design (left cross-section), the first layer is characterized by a larger number of turns that the second layer. The consequent larger accumulated e.m. force determines a peak stress of -243 MPa. By redistributing the number of turns between the two layers (right cross-section) the total e.m. force is shared and the accumulated stress reduced by 30 MPa.

It is important to notice that both designs reach a similar maximum gradient, but the first one is clearly more efficient in term of amount of conductor. In this case, conductor efficiency was sacrificed to improve stress profiles.

Magnet Cross-Section Optimization

Once the coil design is chosen, the following step regards the optimization of the support structure. By providing pre-load to the coil during assembly and cool-down, and counteracting the e.m. forces during excitation, the structure may have a significant impact on the conductor peak stresses. An example is depicted in Fig. 8 and Fig. 9 where the accumulated stress in the coil at maximum field in the LARP quadrupole magnets TQ and LQ are shown. Although both quadrupoles implemented the same coil and operated at the same gradient, a modification of the geometry of the components surrounding the coil implemented in LQ contributed to a 20 MPa reduction of accumulated stress [17].
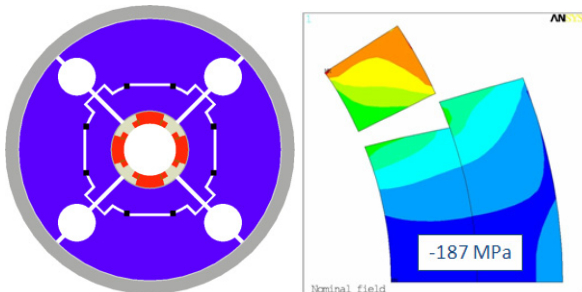

Figure 8: Cross-section of the LARP quadrupole magnet TQ (left) and 2D computations of azimuthal stress with e.m forces (right).
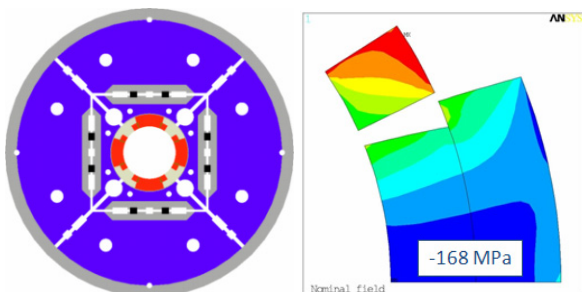

Figure 9: Cross-section of the LARP quadrupole magnet LQ (left) and 2D computations of azimuthal stress with e.m forces (right).

OPTIMIZATION OF COIL FABRICATION PROCESS

The use of finite element magnetic-mechanical models can play an important role also in the optimization of the

coil fabrication process. The models can be focused on investigating the effect of different coil part materials, which must be compatible with the high-temperature heat treatment, at the same time contributing to minimize coil strain during magnet operation. As an example, we present in this section the results of the study, reported in [18-20], regarding the winding poles of the LARP quadrupole magnet TQ.
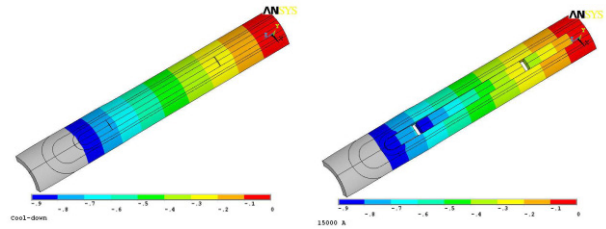

Figure 10: 3D mechanical computations of the deformed shapes (with displacements enhanced by a factor of 50) of the TQ coils after cool-down (left) and at 15 kA (right).
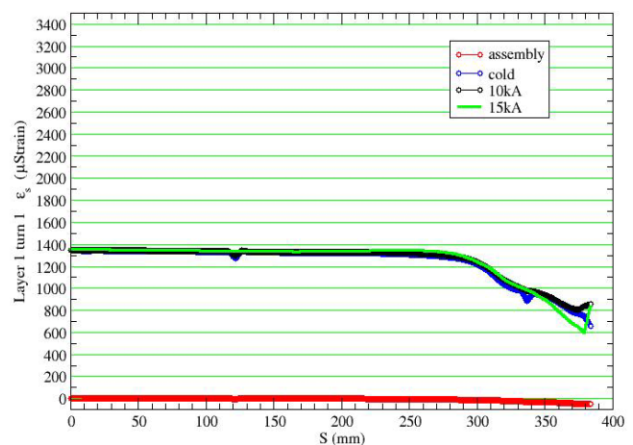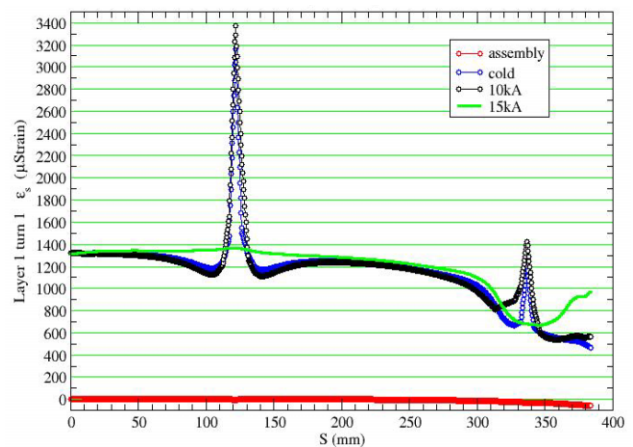

Figure 11: 3D mechanical computations of the pole turn axial strain as a function of the axial position with bronze pole (top) and titanium alloy pole (bottom).

Nb_3Sn coils are usually wound around solid pieces, called poles, which then participate to the full reaction and impregnation process. For fabrication purposes, the winding poles are segmented in several pieces with a length of approximately 200-300 mm. The first set of

Magnets

cos(theta) coils for the TQ quadrupole (TQ01 series) were wound around segmented aluminium bronze poles. During the TQS01 magnet tests, it was observed that quench-origins clustered around the area in between adjacent pole pieces. The numerical simulations indicated that, after cool-down, the segments tend to separate, thus creating gaps which increase during excitation (see deformed shape in Fig. 10). As a result, peaks of axial strain in the pole turn arise in correspondence of the gaps, indicating that the cables around the poles experience high tensions during magnet powering (see Fig 11, top).

This phenomenon was attributed to the friction between the iron components surrounding the coils, characterized by a low thermal contraction coefficient, and the bronze pole pieces, which feature a high thermal contraction coefficient. The friction induces high tension in the bronze poles, which then separate when the e.m. forces were applied. For the second set of coils (TQ02 series) it was therefore decided to change the pole material from bronze to titanium alloy (Ti6Al4V), characterized by a low thermal contraction coefficient: the titanium pole segments remain in compression during all magnet operations, thus eliminating gaps and high strain in the pole turns (see Fig. 11, bottom).

STRAIN AND DISPLACEMENTS IN COIL END REGIONS

Nb_3Sn magnets operating at fields approaching 15 T are subjected to very high axial e.m. forces which stretch the coils along the longitudinal direction. If not counterbalanced, these forces may generate mechanical motions and tensional strain resulting in potential degradation of magnet performance. For these reasons, the LBNL Superconducting Magnet Program has started implementing in the magnet design a coil axial support system based on end plates and aluminium rods (see Fig. 12) with the goal of preventing separation between turns and pole pieces in the end regions. In parallel, 3D models have been focused on mechanical solutions to mitigate the effect of the axial forces.
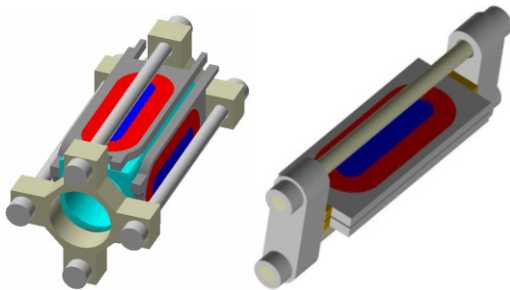

Figure 12: Coil axial supports implemented in the quadrupole SQ (left) and the dipole SD (right).

The importance of the axial support can be seen in Fig. 13, where the model results indicate how the deformation of the turns in the end regions of the TQ quadrupole coils can be significantly reduced by providing sufficient pre-load after cool-down.
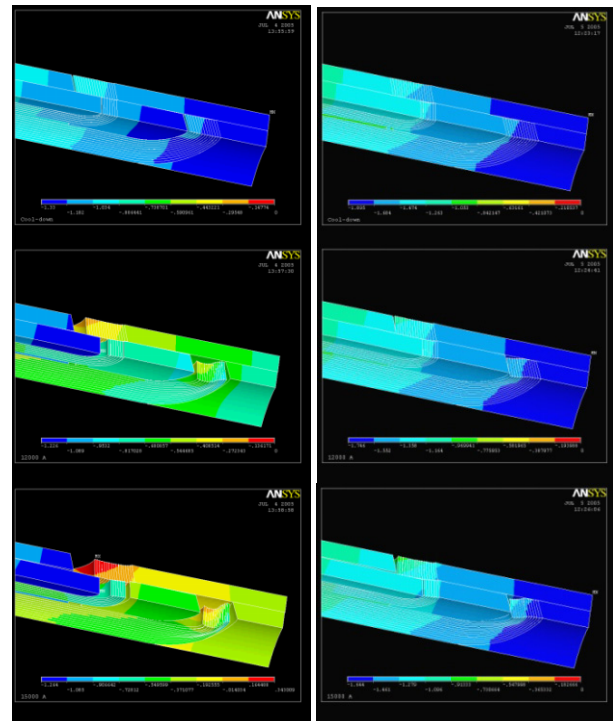

Figure 13: 3D mechanical computations of the deformed shapes (with displ. enhanced by a factor of 50) of the TQ coils without (left) and with (right) axial support after cool-down (top), at 12 kA (centre), and at 15 kA (bottom).

In order to investigate the impact of axial support and prove its effectiveness, in 2007 the LARP program launched a series of tests with the subscale quadrupole magnet SQ02 [21]. The magnet was tested with (SQ02b) and without (SQ02c) axial end load. The training performance is plotted in Fig. 14: the magnet reached its expected current limits when fully supported, but it showed a clear degradation in quench performance (in the order of 5 to 10%) when no axial load was applied: the degradation was progressive over consecutive quenches, i.e., the quench current gradually decreased from 10.2 kA to 9.7 kA in seven quenches.
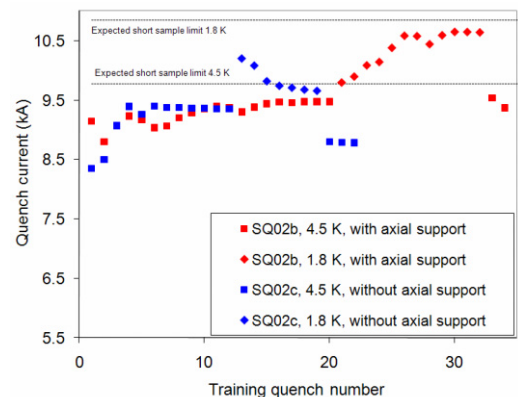

Figure 14: Training performance of SQ02b (at 4.5 K and 1.8 K, with axial support), and SQ02c (at 4.5 K and 1.8 K, without axial support). The dashed lines represent the expected current limits based on strand measurements.

A 3D analysis, reported in [22], pointed out a high tensile strain (about 4500 μstrain) in the cable at the end of the straight section as a probable cause of the performance degradation (Fig. 15).
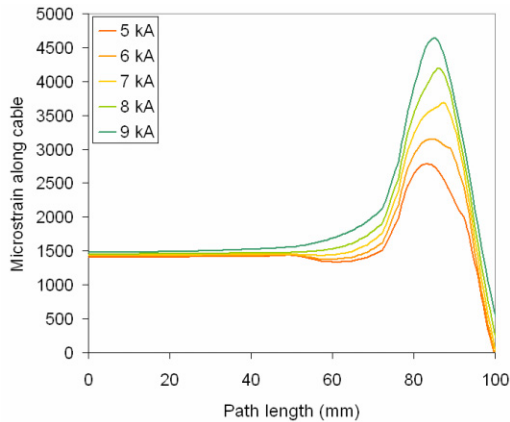

Figure 15: Computed strain during excitation along the cable on a path moving from the centre of the straight section to the end, in the SQ02c conditions.

MODELING OF QUENCH INITIATION AND PROPAGATION

In addition to the increase of strain analyzed in the previous section, the effect of axial e.m. force may include a relative sliding between the pole turns and the winding poles (see deformed shapes in Fig. 16, left). In the presence of friction, any sliding between two surfaces results in energy dissipation.
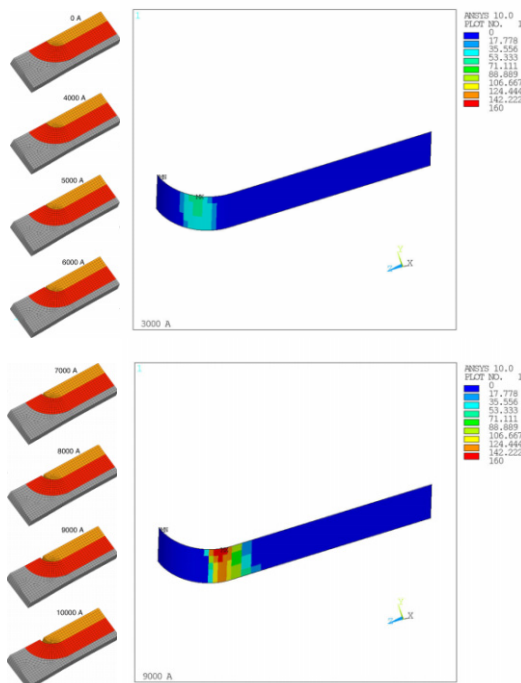

Figure 16: 3D mechanical computations of the deformed shapes (with displ. enhanced by a factor of 50) of the SQ02 coils (left) and frictional energy dissipation [J/m^2] (right) during excitation.

With a 3D finite element model, it is possible to compute the energy dissipation during excitation, and gain useful insight on the areas subjected to premature quenching. This study, reported in [23,24], was performed to analyze the performance of the SQ02 magnet. The results, plotted in Fig. 16, show that, from 0 to 3 kA the release of frictional energy near the end peaks at about 70 J/m^2 (top figure). During the following current steps, the dissipated energy progressively increases to a maximum of 160 J/m^2 (bottom figure) and its location gradually moves towards the straight section. The quench locations recorded during the SQ02a where consistent with the energy dissipation pattern predicted by the model.
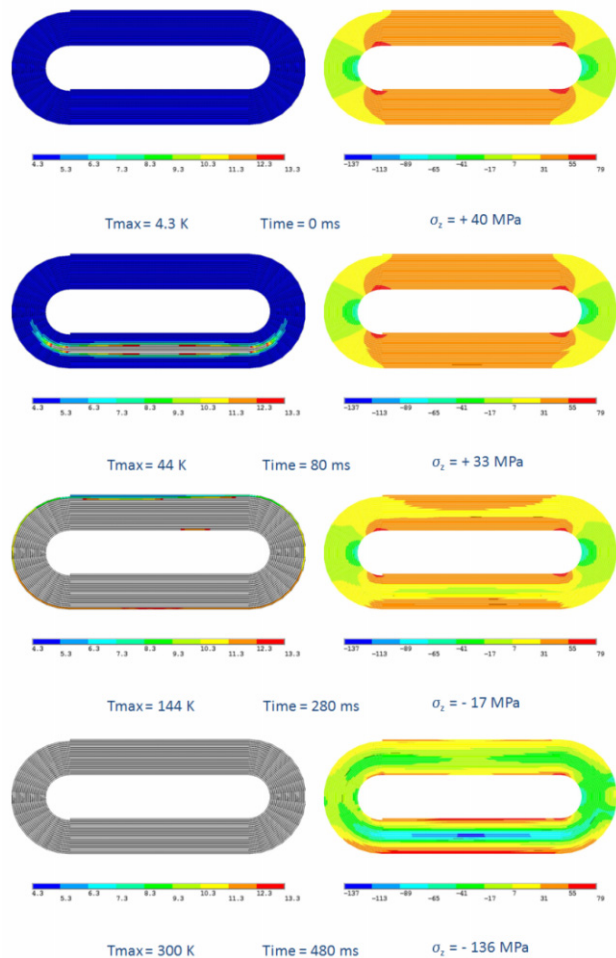

Figure 17: 3D computations of the thermal (K, left) and mechanical (MPa, right) status of the SM coil during quench propagation as a function of time.

If the energy dissipated by a conductor motion is enough to determine an increase of the local temperature of the superconductor beyond its critical level, a quench is originated and starts propagating. After the analysis of quench-triggering mechanisms, the computations can be focused towards a detailed representation of the thermal and mechanical status of a superconducting coil during the propagation of a quench. The goal is to determine the peak temperatures reached by the superconductor and to

extend the analysis to the mechanical response to a quench: the temperature profile evaluated by a thermo-electrical model can be transferred to a 3D mechanical model and the evolution of the coil stresses during the quench propagation investigated.

This analysis, reported in [25] was applied to the SM magnet and is summarized in Fig. 17. The plots on the left of the figure show the propagation of the normal zone (gray area) from quench initiation to 480 ms, when the hot spot temperature reaches a maximum of 300 K. The plots on the right of the figure represent the corresponding stress distribution in the coil. In the hot spot area the coil starts with a longitudinal tension of about 40 MPa before quench propagation. After the quench is initiated, the hotter regions attempt to expand and push against the colder surroundings. The hot spot experiences compression in every direction after the quench, with a maximum compression of about -140 MPa. The study can be used to determine that maximum hot spot temperature allowed in Nb_3Sn superconducting coils before the induced thermal strain degrade the superconductor.

CONCLUSIONS AND NEXT STEPS

The use of the strain-sensitive Nb_3Sn superconductor in the next generation of high-field magnets for particle accelerators will require an in-depth knowledge of the coil mechanical status, which can be obtained only with integrated magnetic, mechanical and thermal design and analysis. We described how a combined use of different tools and techniques allows a full representation of magnet geometry and operation conditions. We then pointed out the importance of focusing the analysis tools on optimizing coil and support structure to minimize coil stress, investigate the strain status of the superconductor from assembly to quench aftermath, and identify and correct quench initiation and training mechanism.
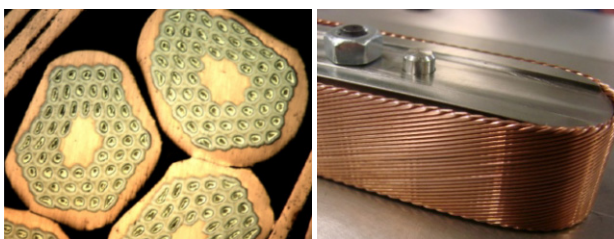

Figure 17: Deformation of strands in the cable edge (left) and cable bending around winding pole (right).

As a next step, we believe that a finer modelling of the mechanical status of the superconductor down to the filament level will constitute a fundamental step to improve our understanding of the behaviour of Nb_3Sn superconducting magnets. To reach this goal, it will be necessary to include in the simulations strand geometries resulting from the coil fabrication process, in particular cabling, winding, reaction and potting (Fig. 17) and implement 2D and 3D models of the Rutherford cable (Fig. 18) capable of reproducing the deformed shape of filaments and strands [26].
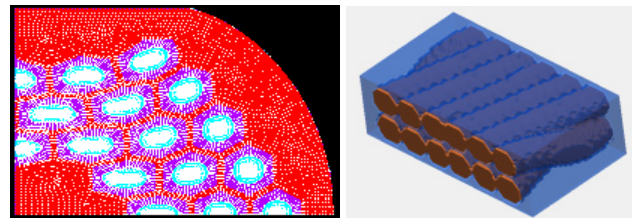

Figure 17: 2D model of a deformed strand (left), and 3D models of a Rutherford cable (right).

REFERENCES

[1] P. Wanderer *et al.,* IEEE Trans. Appl. Supercond., 19 (3), 1122 (2009).

[2] G. de Rijk, CERN 2009-001, 114 (2009).

[3] Godeke *et al,* Supercond. Sci. Techn. 19, R100 (2006).

[4] Dietderich and Godeke, Cryogenics 48, 331 (2008).

[5] S. Caspi and P. Ferracin, IEEE Trans. Appl. Supercond. 16 (2), 1298 (2006).

[6] S. Caspi, P. Ferracin, and S. Gourlay, IEEE Trans. Appl. Supercond. 16 (2), 354 (2006).

[7] L. Rossi and Ezio Todesco Phys. Rev. ST Accel. Beams 9, 102401 (2006).

[8] L. Rossi and Ezio Todesco Phys. Rev. ST Accel. Beams 10, 112401 (2007).

[9] K. Halbach, LLNL report UCRL-17436, 1967.

[10] www.cern.ch/roxie.

[11] Vector Fields Limited, 24 Bankside, Kidlington, Oxford OX5 1JE, England.

[12] ANSYS, Inc., Southpointe, 275 Technology Drive, Canonsburg, PA 15317, USA.

[13] J. Cook, IEEE Trans. Magn. 27 (4), 1976 (1991).

[14] PTC, 140 Kendrick Street, Needham, MA 02494, USA.

[15] H. Felice *et al,* IEEE Trans. Appl. Supercond. 18 (2), 281 (2008).

[16] H. Felice *et al,* IEEE Trans. Appl. Supercond. 19 (3), 1235 (2009).

[17] Paolo Ferracin *et al,* IEEE Trans. Appl. Supercond. 19 (3), 1106 (2009).

[18] S. Caspi *et al,* IEEE Trans. Appl. Supercond. 17 (2), 1122 (2007).

[19] S. Caspi *et al,* IEEE Trans. Appl. Supercond. 18 (2), 179 (2008).

[20] S. Caspi *et al,* IEEE Trans. Appl. Supercond. 19 (3), 1221 (2009).

[21] P. Ferracin *et al,* IEEE Trans. Appl. Supercond. 17 (2), 1019 (2007).

[22] P. Ferracin *et al,* IEEE Trans. Appl. Supercond. 18 (2), 285 (2008).

[23] P. Ferracin *et al,* IEEE Trans. Appl. Supercond. 17 (2), 2373 (2007).

[24] P. Ferracin and S. Caspi, Cryogenics 47 (11-12), 595 (2007).

[25] P. Ferracin *et al,* IEEE Trans. Appl. Supercond. 14 (2), 361 (2004).

[26] D. Arbelaez *et al.*, "Cable Deformation Simulation and a Hierarchical Framework for Nb_3Sn Rutherford Cables", presented at EUCAS 2009.